

Article

Lattice Stability and Elastic Properties of Zr-Ti-X Alloys (X = Al, V) by the First Principles Study

Wenxiong Duan , Xiaoping Liang *, Xiangguan Yang, Yu Wang and Baifeng Luan

College of Materials Science and Engineering, Chongqing University, Chongqing 400030, China; duan116984@163.com (W.D.); caffeine000@foxmail.com (X.Y.); wangyu@cqu.edu.cn (Y.W.); bfluan@cqu.edu.cn (B.L.)

* Correspondence: xplianguan@cqu.edu.cn; Tel.: +86-023-65127306

Received: 6 August 2020; Accepted: 28 September 2020; Published: 1 October 2020



Abstract: Based on a certain ratio of Zr and Ti atomic fractions according to $Zr_{47}Ti_{45}Al_5V_3$ (wt.%), the lattice constants, lattice stability, and elastic properties of Zr-Ti-X alloys (X = Al, V) in body-centered cubic (BCC) (β phase) and hexagonal close-packed (HCP) (α phase) crystal structures were studied using first-principles calculations. It is shown that Al acts as an α stabilizer for Zr-Ti-Al alloys and V can stabilize the β phase for Zr-Ti-V alloys. As the mass fraction of Al increases from 4 wt.% ($Zr_{55}Ti_{41}Al_4$) to 6.8 wt.% ($Zr_{53.2}Ti_{40}Al_{6.8}$), these alloys all have relatively good strength, hardness, and rigidity, however, their ductility deteriorated with the increasing of Al mass fraction. When the mass fraction of V in Zr-Ti-V alloys is 2.4 wt.%, $Zr_{55.6}Ti_{42}V_{2.4}$ (wt.%) achieved the best strength, hardness, and rigidity, when the mass fraction of V increases from 0 ($Zr_{57}Ti_{43}$) to 12 wt.% ($Zr_{50.2}Ti_{37.8}V_{12}$), their ductility improved. The changes of phase compositions and structure with Al content or V content distinctly affect mechanical properties of ternary Zr-Ti-X alloys (X = Al, V), the amount of Zr and Ti could be factors that impact the mechanical properties of the multiphase $Zr_{47}Ti_{45}Al_5V_3$ from the point of view of ternary Zr-Ti-Al and Zr-Ti-V compositions.

Keywords: first principles; mass fraction; lattice stability; elastic properties

1. Introduction

In recent decades, with the increasing number of spacecraft launched by various countries, the space environment has become increasingly complex, and the development of high-performance structural materials suitable for the space environment has become an inevitable choice for the spacecraft in the future [1–4]. For the critical components and structural parts of spacecraft, high-strength steel with higher density is the main material commonly utilized in the past, but the application of traditional steel is greatly restricted because of the demand for lightweight spacecraft. Therefore, there is an urgent need to develop high-strength and lightweight materials suitable for spacecraft structural parts. Many studies have shown that titanium alloys are expected to replace high-strength steel as critical components and structural materials in spacecraft, all because of their low density, high specific strength, good corrosion resistance, and low temperature performance [5–7]. Among hundreds of titanium alloys, $Ti_{90}Al_6V_4$ (wt.%) is widely used owing to its excellent mechanical performance. However, the service life of $Ti_{90}Al_6V_4$ (wt.%) will be greatly reduced because of poor impact resistance in the face of space debris, narrow working parameter range, complex manufacturing processes, as well as large deformation, and high strain rate at high temperature, if it is applied to spacecraft structural parts [8–10]. As is known to all that adding different elements to the alloys can greatly affect the lattice stabilities and mechanical properties of the alloys [11–14], therefore, it is expected to enhance the applicability of $Ti_{90}Al_6V_4$ (wt.%) in space by adding alloying elements. In 2012, from the perspective of adding zirconium element to $Ti_{90}Al_6V_4$ (wt.%), Jing et al. developed a new type of

alloy— $Zr_{47}Ti_{45}Al_5V_3$ (wt.%) [15]. The chemical properties of Zr and Ti are similar because these elements belong to the same primary group (IVB), have two kinds of crystal structure (α - and β -type), and can form an infinitely miscible solid solution [16]. Compared with $Ti_{90}Al_6V_4$ (wt.%), $Zr_{47}Ti_{45}Al_5V_3$ (wt.%) has great mechanical properties. The hardness of $Zr_{47}Ti_{45}Al_5V_3$ (wt.%) is above 400 HV, which is nearly 30% higher than $Ti_{90}Al_6V_4$ (wt.%). Its material strength after heat treatment is above 1400 MPa, and its density is only about 2/3 of high-strength steel [17], thus, $Zr_{47}Ti_{45}Al_5V_3$ (wt.%) is a new type of alloy with great potential.

Since the $Zr_{47}Ti_{45}Al_5V_3$ (wt.%) was proposed, there are research findings which reported the relation of macroscopic rheological characteristic with microstructures of $Zr_{47}Ti_{45}Al_5V_3$ (wt.%) subjected to hot tensile, compression, or torsion deformation. In 2012, Liang et al. [16] studied the structural and mechanical properties of hot-rolled Zr-Ti-Al-V alloys based on X-ray diffraction and metallographic analyses. Results showed that the microstructure of alloys went through a series of changes from the α (α')-phase to part or all of the β -phase, thus affecting the mechanical properties as Zr increased. In 2013, Liang et al. [18] experimentally studied the effect of Al content on the microstructure and mechanical properties of hot rolled $Zr_{47}Ti_{45}Al_5V_3$ (wt.%), results showed that the Zr-Ti-Al-V alloys with Al contents between 3.3 wt.% and 5.6 wt.% have excellent mechanical properties. Zhang et al. [19] conducted impact compression experiments on $Zr_{47}Ti_{45}Al_5V_3$ (wt.%), and results showed that no obvious evidence of phase transition is found in the shock compression pressure range. In 2016, Tan et al. [20] studied the hot deformation behavior of $Zr_{47}Ti_{45}Al_5V_3$ (wt.%) with an initial lamellar α -phase structure through a compression test in the temperature range of 823 K to 1073 K, researches showed that the flow curves exhibited a continuous flow softening in the $\alpha + \beta$ phase field. Liang et al. [21] investigated the effects of V content (0–7 wt.%) on the structure and mechanical properties of Zr-Ti-Al-V alloys, and results showed that the phase composition changes as $\alpha' \rightarrow \alpha' + (\alpha'' + \beta) \rightarrow \alpha'' + \beta \rightarrow \beta + (\alpha'') \rightarrow \beta$ with increased V content from 0 wt.% to 7 wt.%, and the elastic modulus and yield strength show an antiparabolic trend with increased V content. In 2018, Tan et al. [22] studied the effect of thermal deformation on the $\alpha \rightarrow \beta$ phase transition of $Zr_{47}Ti_{45}Al_5V_3$ (wt.%), results showed that with decreasing strain rate and increasing deformation temperature, the volume fraction and size of globular α phase increased.

At present, most of the research [23–25] on experimental methods discussed the influence of alloy processing technology on structure and mechanical properties. For Zr-Ti-Al-V alloys, there is a lack of in-depth research about the effect of element composition and phase structure on their mechanical properties. However, mastering the relation between the element composition, phase structure, and mechanical properties is an effective way to optimize the alloy properties [26–32], and it is of great significance to study the lattice stabilities and elastic properties of Zr-Ti-Al-V alloy systems. Marker et al. [33] studied the elastic properties of the Zr-Ti-X (X = Nb, Sn, Ta) alloys in the BCC structure, and predicted the single crystal elastic stiffness coefficients and polycrystalline aggregate properties using DFT-based first-principles calculations. Liao et al. [34] established the single-crystal elastic constant model of the quaternary BCC Zr-Ti-Nb-V alloys across full composition space using first principles, based on the research of Marker et al. [33], the accuracy of the model was confirmed by comparing with previous calculations and experiments. Konopatsky et al. [35] carried out the multi-cycle mechanical testing on ternary $Ti_{68}Zr_{18}Nb_{14}$ (at.%), quaternary $Ti_{68}Zr_{18}Nb_{13}Ta_1$ (at.%), $Ti_{68}Zr_{18}Nb_{12}Ta_2$ (at.%), and $Ti_{68}Zr_{18}Nb_{11}Ta_3$ (at.%) alloys, during multi-cycle mechanical testing, the following regularity appeared for all the alloys tested: during 10–15 first loading-unloading cycles, the mechanisms of plastic deformation and stress-induced martensite formation and stabilization prevail.

Many researchers have proved that phase composition of the Zr-Ti-Al-V alloys significantly depends on the amount of Zr and Ti [16], and changes of phase compositions and structure with alloying element distinctly affected mechanical properties of Zr-Ti-Al-V alloys [21]. It is of great significance to study the alloying effects of Al and V to provide guidance for further optimizing the lattice stabilities and mechanical properties regulation of quaternary $Zr_{47}Ti_{45}Al_5V_3$ (wt.%), in other words, the research of alloying element content could provide direction and assistance in guiding the research of quaternary alloys from the point of view of ternary alloys.

In this paper, we performed first-principles studies of Zr-Ti-X ($X = \text{Al}, \text{V}$) alloys using the special quasi-random structure (SQS) models to explore the relationship between element composition, phase structure, lattice stabilities, and elastic properties based on previous studies [36]. This article starts from the basic composition of $\text{Zr}_{47}\text{Ti}_{45}\text{Al}_5\text{V}_3$ (wt.%), the lattice constants, total energies, and elastic constants of the Zr-Ti-X ($X = \text{Al}, \text{V}$) alloys are calculated. These calculations provide an effective guide for further optimizing the composition of the Zr-Ti-X ($X = \text{Al}, \text{V}$) alloys, and provide guidance and help in exploring the complex relationship between the ternary alloys and quaternary alloys.

2. Materials and Methods

Based on the ratio of the Zr atomic fraction and the Ti atomic fraction in the $\text{Zr}_{47}\text{Ti}_{45}\text{Al}_5\text{V}_3$ (wt.%), in order to investigate the effect of alloying elements Al and V on the crystal structures and mechanical properties of $\text{Zr}_{47}\text{Ti}_{45}\text{Al}_5\text{V}_3$ (wt.%) alloy, two types of ternary alloy systems were designed—Zr-Ti-Al alloy systems and Zr-Ti-V alloy systems. For these two types of alloy systems, the hcp and bcc structures were studied to model α and β phase because a mixture of two phases usually appears in these alloys, which gives a better understanding of the phase properties of two competitive phases. In this paper, the special quasi-random structure (SQS) method was used in the alloy systems with hexagonal close-packed structure (HCP, α phase) and body-centered cubic structure (BCC, β phase).

To simplify the calculation, the atomic ratio of Zr and Ti is approximately 0.35:0.50. Figure 1 shows the SQS model of the $\text{Zr}_{35}\text{Ti}_{50}\text{Al}_{15}$ (at.%) alloys in HCP structure and BCC structure used in modeling in this article; the SQS model of the $\text{Zr}_{35}\text{Ti}_{50}\text{V}_{15}$ (at.%) alloys in HCP structure and BCC structure is shown in Figure 2. Table 1 shows the $\text{Zr}_y\text{Ti}_z\text{Al}_{100-(y+z)}$ (at.%) alloys ($y:z = 0.35:0.50$, and the atomic fraction of Al goes from 0 to 15 at.% with a gradient of 3 at.%) in HCP and BCC structures. Table 2 shows the $\text{Zr}_y\text{Ti}_z\text{V}_{100-(y+z)}$ alloys (at.%) ($y:z = 0.35:0.50$, and the atomic fraction of V goes from 0 to 15 at.% with a gradient of 3 at.%) in HCP and BCC structures. In this paper, the randomness of atomic configuration was reproduced while considering the local relaxation in the supercell through modeling.

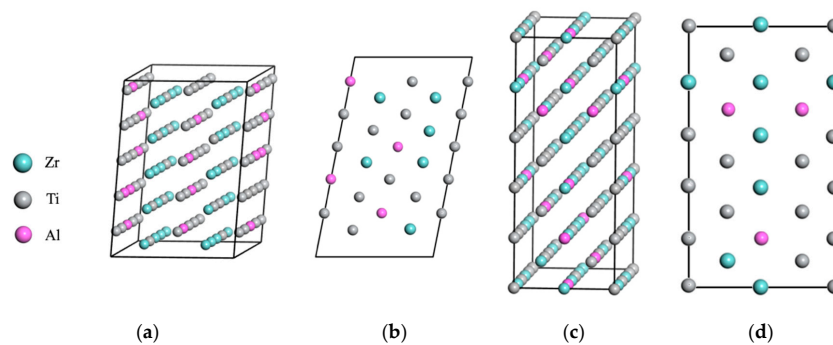


Figure 1. Special quasi-random structure (SQS) model of $\text{Zr}_{35}\text{Ti}_{50}\text{Al}_{15}$ (at.%) alloys: (a) hexagonal close-packed (HCP) structure in 3D; (b) HCP structure in 2D; (c) body-centered cubic (BCC) structure in 3D; (d) BCC structure in 2D.

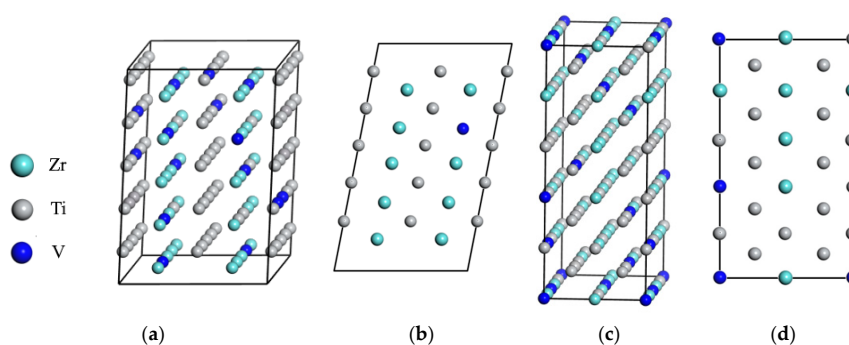


Figure 2. SQS model of $\text{Zr}_{35}\text{Ti}_{50}\text{V}_{15}$ (at.%) alloys: (a) HCP structure in 3D; (b) HCP structure in 2D; (c) BCC structure in 3D; (d) BCC structure in 2D.

Table 1. Zr-Ti-Al alloy systems in HCP structure and BCC structure with different atomic fraction of Al.

Structures	System	Composition (at.%)
HCP	Zr-Ti-Al	Zr ₄₁ Ti ₅₉
		Zr ₄₀ Ti ₅₇ Al ₃
		Zr ₃₉ Ti ₅₅ Al ₆
		Zr ₃₈ Ti ₅₃ Al ₉
		Zr ₃₆ Ti ₅₂ Al ₁₂
		Zr ₃₅ Ti ₅₀ Al ₁₅
BCC	Zr-Ti-Al	Zr ₄₁ Ti ₅₉
		Zr ₄₀ Ti ₅₇ Al ₃
		Zr ₃₉ Ti ₅₅ Al ₆
		Zr ₃₈ Ti ₅₃ Al ₉
		Zr ₃₆ Ti ₅₂ Al ₁₂
		Zr ₃₅ Ti ₅₀ Al ₁₅

Table 2. Zr-Ti-V alloy systems in HCP structure and BCC structure with different atomic fraction of V.

Structures	System	Composition (at.%)
HCP	Zr-Ti-V	Zr ₄₁ Ti ₅₉
		Zr ₄₀ Ti ₅₇ V ₃
		Zr ₃₉ Ti ₅₅ V ₆
		Zr ₃₈ Ti ₅₃ V ₉
		Zr ₃₆ Ti ₅₂ V ₁₂
		Zr ₃₅ Ti ₅₀ V ₁₅
BCC	Zr-Ti-V	Zr ₄₁ Ti ₅₉
		Zr ₄₀ Ti ₅₇ V ₃
		Zr ₃₉ Ti ₅₅ V ₆
		Zr ₃₈ Ti ₅₃ V ₉
		Zr ₃₆ Ti ₅₂ V ₁₂
		Zr ₃₅ Ti ₅₀ V ₁₅

In this article, the CASTEP (Cambridge Sequential Total Energy Package, Cambridge, UK) total energy calculation software package, based on the density functional theory (DFT) [37] pseudopotential plane wave method [38], was used to analyze the Zr-Ti-Al alloys and Zr-Ti-V alloys in HCP and BCC structures for first-principles calculations. Density functional theory (DFT) as an effective approximation method is used to solve the structure of multi-electronic systems [39–46], and it obtains the total energy of multi-electronic systems based on the energy minimization method. The pseudopotentials describe the valence configurations of the elements, which are as follows: Zr 4s²4p⁶4d²5s², Ti 3s²3p⁶3d²4s², Al 3s²3p¹ and V 3s²3p⁶3d³4s². The electronic exchange–correlation energy was treated within the generalized gradient approximation (GGA) with the PBE revised for solids [47]. The convergence criteria of 5 × 10^{−7} eV per atom was applied to be self-consistent, all calculations were executed in reciprocal space to improve the speed and accuracy, in addition, the calculation and convergence were controlled by the cut-off point of the wave energy of the Ultrasoft pseudopotential plane. After convergence is tested, the Monkhorst-Pack grid of 2 × 2 × 3 is adopted for the brillouin zone integration, the plane wave kinetic energy cut-off was determined as 350 eV, and the unit cell parameters of Zr-Ti-Al alloys and Zr-Ti-V alloys are calculated by first principles. About the lattice stability, formation energy $E_f(\text{Zr}_y\text{Ti}_z\text{X}_{100-(y+z)})$ was defined by:

$$E_f(\text{Zr}_y\text{Ti}_z\text{X}_{100-(y+z)}) = \{E(\text{Zr}_y\text{Ti}_z\text{X}_{100-(y+z)}) - yE(\text{Zr}) - zE(\text{Ti}) - [100 - (y + z)]E(\text{X})\} / 100 \quad (1)$$

Here, $E(\text{Zr}_y\text{Ti}_z\text{X}_{100-(y+z)})$ is the total energy per atom of the $\text{Zr}_y\text{Ti}_z\text{X}_{100-(y+z)}$ (at.%) alloy with alloying element concentration. $E(\text{Zr})$, $E(\text{Ti})$, and $E(\text{X})$ are the energies per atom of Zr, Ti, and X in their ground state structures.

In this paper, according to our modeling system based on static modeling, the total energy and forming energy of the system calculated in this paper are considered from the level of electron exchange. They are themselves relative values because most of the energy is subtracted based on mass–energy equivalence. The energy of the atom itself is approximated as the absolute value of the total non-electron energy, which may not be considered in this article. We performed a static total energy calculation, based on that, the lattice stabilities of Zr-Ti-X (X = Al, V) alloys are evaluated with analyzing the total energy dependence on elements species, alloying fraction, and phase structure using the first principles in our work.

We determined the independent elastic coefficients, C_{ij} , based on expanding the total energy, U , of the crystal as a function of lattice strain ϵ [48], which is expressed as

$$U = U_0 + V \sum_i \sigma_i \epsilon_i + \frac{1}{2} V \sum_i \sum_j C_{ij} \epsilon_i \epsilon_j + \dots \quad (2)$$

where V is the volume and U_0 is the total energy of the undistorted lattice system. The linear term in the expansion vanished, and the cubic or higher powers of ϵ_i terms in the polynomial expansion are neglected for sufficiently small strains.

In this paper, the elastic constant, C_{ij} , that describes the response of the crystal to external forces, is generally used to determine the strength of a material [49]. Based on the research findings of Zhou et al. [50], we theoretically predicted the elastic properties of Zr-Ti-X (X = Al, V) alloys of the alloying elements.

A small strain (δ) is applied to the solid lattice of the $Zr_y Ti_z V_{100-(y+z)}$ (at.%) alloys to construct a quadratic function relationship between the total energy changes (ΔU) and the strains (δ) according to the Hooks law, as follows:

$$\Delta U = \frac{V}{2} \sum_{i,j=1}^6 C_{ij} \epsilon_i \epsilon_j \quad (3)$$

where ΔU is the total energy changes, V is the original unit cell volume, C_{ij} are the elastic constants, ϵ_i and ϵ_j are the components of strain matrix.

In order to investigate these elastic constants, as shown in Table 3, three sets of specific strains (δ) are applied to BCC metal in different directions. We also list the different strain configurations to compute the five independent elastic constants of HCP metal in Table 4. The elastic constants can be obtained by fitting the relationship between the total energy changes (ΔU) and the applied strains (δ).

Table 3. The relationship between the strains (δ) and the total energy changes (ΔU) of BCC metal.

Strain	Change of Total Energy
$\epsilon = (0, 0, 0, \delta, \delta, \delta)$	$\frac{\Delta U}{V} = \frac{3}{2} C_{44} \delta^2$
$\epsilon = (\delta, \delta, 0, 0, 0, 0)$	$\frac{\Delta U}{V} = (C_{11} + C_{12}) \delta^2$
$\epsilon = (\delta, \delta, \delta, 0, 0, 0)$	$\frac{\Delta U}{V} = \frac{3}{2} (C_{11} + 2C_{12}) \delta^2$

Table 4. The relationship between the strains (δ) and the total energy changes (ΔU) of HCP metal.

Strain	Change of Total Energy
$\epsilon = (\delta, \delta, 0, 0, 0, 0)$	$\frac{\Delta U}{V} = (C_{11} + C_{12}) \delta^2$
$\epsilon = (0, 0, 0, 0, 0, \delta)$	$\frac{\Delta U}{V} = \frac{1}{4} (C_{11} - C_{12}) \delta^2$
$\epsilon = (0, 0, \delta, 0, 0, 0)$	$\frac{\Delta U}{V} = \frac{1}{2} C_{33} \delta^2$
$\epsilon = (0, 0, 0, \delta, \delta, 0)$	$\frac{\Delta U}{V} = C_{44} \delta^2$
$\epsilon = (\delta, \delta, \delta, 0, 0, 0)$	$\frac{\Delta U}{V} = \frac{3}{2} (C_{11} + 2C_{12}) \delta^2$

For different unit cell structures, the stability criteria are also different according to Born-Huang's mechanical stability theory. In this paper, the HCP Zr-Ti-Al alloys and HCP Zr-Ti-V alloys are calculated by first principles to obtain five independent elastic constants, C_{11} , C_{12} , C_{13} , C_{33} , and C_{44} , their stability is determined from the elastic constants by:

$$C_{11} > 0 \quad (4)$$

$$C_{44} > 0 \quad (5)$$

$$C_{11} > C_{12} \quad (6)$$

$$(C_{11} + C_{12})C_{33} - 2C_{13}^2 > 0 \quad (7)$$

The BCC Zr-Ti-Al alloy systems and BCC Zr-Ti-V alloy systems are calculated by first principles to obtain three independent elastic constants, C_{11} , C_{12} and C_{44} , their stability is determined from the elastic constants by:

$$C_{11} + 2C_{12} > 0 \quad (8)$$

$$C_{11} > C_{12} \quad (9)$$

$$C_{44} > 0 \quad (10)$$

The mechanical parameters of the Zr-Ti-Al alloys and Zr-Ti-V alloys can be calculated by using single crystal elastic constants according to the Voigt-Reuss-Hill scheme [51–54]. The bulk modulus (B), shear modulus (G), Young's modulus (E), and Poisson's ratio (ν) of the Zr-Ti-Al alloys and Zr-Ti-V alloys are calculated as follows:

$$B_V = \frac{1}{9}(C_{11} + C_{22} + C_{33}) + \frac{2}{9}(C_{12} + C_{13} + C_{23}) \quad (11)$$

$$\frac{1}{B_R} = (S_{11} + S_{22} + S_{33}) + 2(S_{12} + S_{13} + S_{23}) \quad (12)$$

$$B_H = \frac{B_R + B_V}{2} \quad (13)$$

$$G_V = \frac{1}{15}(C_{11} + C_{22} + C_{33}) - \frac{1}{15}(C_{12} + C_{13} + C_{23}) - \frac{1}{5}(C_{44} + C_{55} + C_{66}) \quad (14)$$

$$\frac{15}{G_R} = 4(S_{11} + S_{22} + S_{33}) - 4(S_{12} + S_{13} + S_{23}) + 3(S_{44} + S_{55} + S_{66}) \quad (15)$$

$$G_H = \frac{G_V + G_R}{2} \quad (16)$$

$$E = \frac{9B_H G_H}{3B_H + G_H} \quad (17)$$

$$\nu = \frac{3B_H - 2G_H}{2(3B_H + G_H)} \quad (18)$$

The ratio of bulk modulus to shear modulus (B_H/G_H) proposed by Pugh [55] has been widely used to evaluate the toughness and brittleness of materials. It should be noted that a lower value of B means the atomic bond is weaker. Consequently, materials with a low value of B exhibit relatively poor resistance to various forms of localized corrosion (such as intergranular corrosion, pitting corrosion and stress-corrosion cracking) [56–58]. Furthermore, Clerc et al. [59] have demonstrated that the hardness of the annealed metal is proportional to G. It is commonly known that materials with a high value of the B/G ratio (>1.75) often result in ductility, while materials with a low value of the B/G ratio (<1.75) often exhibit brittleness [56,58,60,61]. Vitos et al. investigated the elastic properties of the

$\text{Fe}_{100-(c+n)}\text{Cr}_c\text{Ni}_n$ alloys (13.5 at.% < c < 25.5 at.% and 8 at.% < n < 24 at.%) [56], in that work, shear modulus (G) and bulk modulus (B) fall into the range of 74–81 GPa and 161–178 GPa, respectively.

In addition, the brittleness and ductility of materials can also be judged according to the value of Poisson's ratio ν and the Cauchy pressure, that is, the difference between C_{12} and C_{44} [62]. The larger the value of Poisson's ratio ν , the better the ductility of the material, and if the calculated Cauchy pressure of materials is negative or their Poisson's ratio ν is lower than 0.26, these materials can be considered brittle. Jiang et al. [63] investigated the mechanical properties and Debye temperature of W-TM (TM = Cr, Cu, Fe, Mn, Mo, and Ni, respectively) alloys based on the first principles method, and results showed that the ductile/brittle properties of W-TM alloys can be evaluated based on the mechanical characteristic of B/G ratio, Poisson's ratio (ν), and Cauchy pressure (C').

3. Results and Discussion

Single cell unit cell parameters of alloy systems are shown in Section 3.1. In Section 3.2, the lattice stability of Zr-Ti-X ($X = \text{Al}, \text{V}$) alloys are evaluated with analyzing the total energy dependence on elements species, alloying fraction, and phase structure. The elastic constants of BCC and HCP Zr-Ti-X ($X = \text{Al}, \text{V}$) alloys, are shown in Section 3.3. Finally, the bulk modulus (B), shear modulus (G), Young's modulus (E), and Poisson's ratio (ν) of BCC and HCP Zr-Ti-X ($X = \text{Al}, \text{V}$) alloys are then examined.

3.1. Lattice Constants

The calculated lattice constants a , b , and c (Å) for HCP-structured and BCC-structured Zr-Ti-Al alloy systems with different Al atomic fractions are shown in Table 5, the single crystal cell parameters for HCP-structured and BCC-structured Zr-Ti-V alloy systems with various V concentrations are listed in Table 6.

Considering the concentration dependence, the lattice parameters decrease with increasing Al and V content, and the lattice parameters of the Zr-Ti-Al alloys and Zr-Ti-V alloys are close to each other.

Table 5. Effect of Al atomic fraction on single crystal cell parameters of HCP structure and BCC structure Zr-Ti-Al alloy systems.

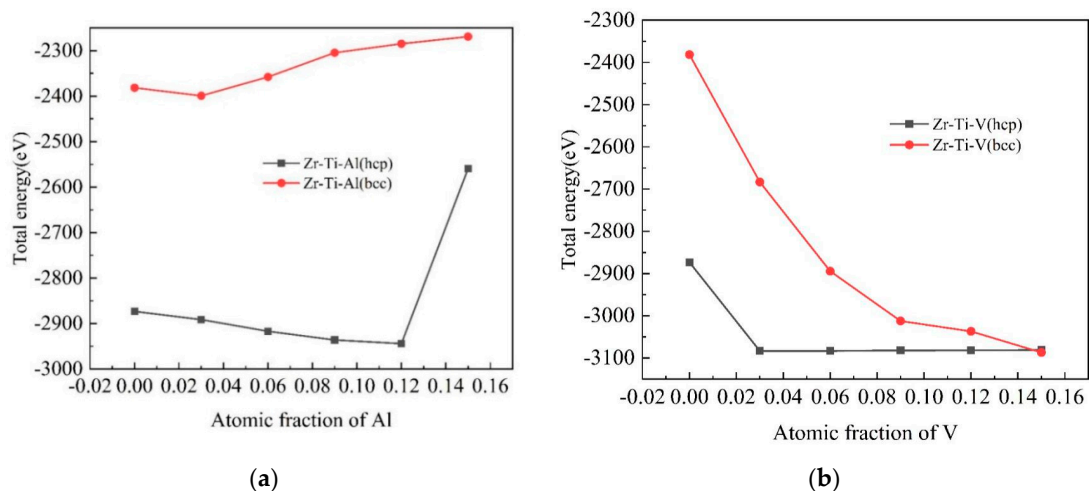
Structures	System	Composition (at.%)	Lattice Parameters (Å)		
			a	b	c
HCP	Zr-Ti-Al	Zr ₄₁ Ti ₅₉	3.039	3.039	4.924
		Zr ₄₀ Ti ₅₇ Al ₃	3.028	3.028	4.873
		Zr ₃₉ Ti ₅₅ Al ₆	3.012	3.012	4.825
		Zr ₃₈ Ti ₅₃ Al ₉	2.993	2.993	4.763
		Zr ₃₆ Ti ₅₂ Al ₁₂	2.982	2.982	4.689
		Zr ₃₅ Ti ₅₀ Al ₁₅	2.971	2.971	4.597
BCC	Zr-Ti-Al	Zr ₄₁ Ti ₅₉	3.382	3.382	3.382
		Zr ₄₀ Ti ₅₇ Al ₃	3.368	3.368	3.368
		Zr ₃₉ Ti ₅₅ Al ₆	3.354	3.354	3.354
		Zr ₃₈ Ti ₅₃ Al ₉	3.341	3.341	3.341
		Zr ₃₆ Ti ₅₂ Al ₁₂	3.333	3.333	3.333
		Zr ₃₅ Ti ₅₀ Al ₁₅	3.325	3.325	3.325

Table 6. Effect of V atomic fraction on single crystal cell parameters of HCP structure and BCC structure Zr-Ti-V alloy systems.

Structures	System	Composition (at.%)	Lattice Parameters (Å)		
			a	b	c
HCP	Zr-Ti-V	Zr ₄₁ Ti ₅₉	3.039	3.039	4.924
		Zr ₄₀ Ti ₅₇ V ₃	3.029	3.029	4.878
		Zr ₃₉ Ti ₅₅ V ₆	3.014	3.014	4.831
		Zr ₃₈ Ti ₅₃ V ₉	2.998	2.998	4.772
		Zr ₃₆ Ti ₅₂ V ₁₂	2.989	2.989	4.694
		Zr ₃₅ Ti ₅₀ V ₁₅	2.978	2.978	4.622
BCC	Zr-Ti-V	Zr ₄₁ Ti ₅₉	3.382	3.382	3.382
		Zr ₄₀ Ti ₅₇ V ₃	3.371	3.371	3.371
		Zr ₃₉ Ti ₅₅ V ₆	3.359	3.359	3.359
		Zr ₃₈ Ti ₅₃ V ₉	3.346	3.346	3.346
		Zr ₃₆ Ti ₅₂ V ₁₂	3.338	3.338	3.338
		Zr ₃₅ Ti ₅₀ V ₁₅	3.329	3.329	3.329

3.2. Lattice Stability

As shown in Figure 3, the lattice stability of Zr-Ti-X (X = Al, V) alloys are evaluated with analyzing the total energies dependence on elements species, alloying fraction and phase structure using the first principles. Lattice stability studies are carried out with the purpose of explaining the complex relationships between the mechanical properties and the alloying elements, deformation, and temperature.

**Figure 3.** (a) Effect of Al atom fraction on total energy of Zr-Ti-Al alloy systems; (b) effect of V atom fraction on total energy of Zr-Ti-V alloy systems.

As shown in Figure 3a, the Zr-Ti-Al alloys in BCC structure generally have higher total energy than HCP Zr-Ti-Al alloys, and the introduction of Al atoms does not change the fact that the HCP Zr-Ti alloys is more stable than BCC [36]. When the Al atomic fraction reaches about 12 at.%, that is, when the Al mass fraction reaches about 5 wt.%, the HCP Zr-Ti-Al alloys are the most stable because of the lowest total energy, while their stability will decrease if the Al atomic fraction continues to increase. For the Zr-Ti-Al alloys in BCC structure, the introduction of Al atoms will enhance the stability because of micro alloying. When the mass fraction of Al goes from 0 to 1 wt.%, the structural stability of BCC Zr-Ti alloys will be improved, and reach the maximum when the mass fraction of Al is about 1 wt.%, but their stability will gradually decrease after the mass fraction of Al exceeds 1 wt.%. Therefore, the Al

element can be regarded as a stable element of α phase of Zr-Ti alloys, which verifies the experimental research of Cordeiro [64].

It can be seen in Figure 3b, the introduction of V atoms can greatly enhance the stability of BCC-structured Zr-Ti alloys. When the V atomic fraction reaches about 15 at.%, the total energies of the BCC Zr-Ti-V alloys are lower than that of the HCP Zr-Ti-V alloys. For the HCP-structured Zr-Ti alloys, because of the micro alloying effect brought by trace V elements, their stability will be enhanced. But when the V atomic fraction exceeds 3 at.%, the continued addition of V atoms has little effect on the structural stability of HCP Zr-Ti-V alloys. In addition, the increase of V atomic fraction will greatly improve the structural stability of BCC Zr-Ti-V alloys. Thus, the V element can be regarded as a stable element of β phase in the Zr-Ti alloys, which also verifies the experimental research of Cordeiro [64].

3.3. Elastic Properties

In this study, the elastic constants of Zr-Ti-Al alloy systems (Table 7) in HCP structure and BCC structure and Zr-Ti-V alloy systems (Table 8) in HCP structure and BCC structure were calculated by first principles. Figure 4 shows the effect of Al atomic fraction on the independent elastic constants of HCP-structured and BCC-structured Zr-Ti-Al alloy systems, Figure 5 shows the effect of V atomic fraction on the independent elastic constants of HCP-structured and BCC-structured Zr-Ti-V alloy systems.

Table 7. Independent elastic constants of HCP structure and BCC structure Zr-Ti-Al alloy systems.

Structures	System	Composition (at.%)	Elastic Constants/GPa					
			C ₁₁	C ₁₂	C ₁₃	C ₃₃	C ₄₄	C ₆₆
HCP	Zr-Ti-Al	Zr ₄₁ Ti ₅₉	178.1	45.2	70.1	184.2	27.1	65.8
		Zr ₄₀ Ti ₅₇ Al ₃	183.4	46.1	72.3	189.5	27.6	66.3
		Zr ₃₉ Ti ₅₅ Al ₆	189.2	46.8	75.4	192.3	28.2	66.8
		Zr ₃₈ Ti ₅₃ Al ₉	191.4	47.5	77.9	198.2	28.5	67.2
		Zr ₃₆ Ti ₅₂ Al ₁₂	194.5	47.9	79.3	203.3	28.9	67.5
		Zr ₃₅ Ti ₅₀ Al ₁₅	201.1	48.4	82.8	205.9	32.5	68.1
BCC	Zr-Ti-Al	Zr ₄₁ Ti ₅₉	118.3	94.7	\	\	33.6	\
		Zr ₄₀ Ti ₅₇ Al ₃	119.5	95.4	\	\	35	\
		Zr ₃₉ Ti ₅₅ Al ₆	120.2	95.8	\	\	36.3	\
		Zr ₃₈ Ti ₅₃ Al ₉	121.8	96.2	\	\	38.5	\
		Zr ₃₆ Ti ₅₂ Al ₁₂	122.2	97.9	\	\	39.1	\
		Zr ₃₅ Ti ₅₀ Al ₁₅	123.6	99.3	\	\	40.5	\

Table 8. Independent elastic constants of HCP structure and BCC structure Zr-Ti-V alloy systems.

Structures	System	Composition (at.%)	Elastic Constants/GPa					
			C ₁₁	C ₁₂	C ₁₃	C ₃₃	C ₄₄	C ₆₆
HCP	Zr-Ti-V	Zr ₄₁ Ti ₅₉	178.1	45.2	70.1	184.2	27.1	65.8
		Zr ₄₀ Ti ₅₇ V ₃	183.4	46.1	72.3	189.5	27.6	66.3
		Zr ₃₉ Ti ₅₅ V ₆	189.2	46.8	75.4	192.3	28.2	66.8
		Zr ₃₈ Ti ₅₃ V ₉	191.4	47.5	77.9	198.2	28.5	67.2
		Zr ₃₆ Ti ₅₂ V ₁₂	194.5	47.9	79.3	203.3	28.9	67.5
		Zr ₃₅ Ti ₅₀ V ₁₅	201.1	48.4	82.8	205.9	32.5	68.1
BCC	Zr-Ti-V	Zr ₄₁ Ti ₅₉	118.3	94.7	\	\	33.6	\
		Zr ₄₀ Ti ₅₇ V ₃	119.5	95.4	\	\	35	\
		Zr ₃₉ Ti ₅₅ V ₆	120.2	95.8	\	\	36.3	\
		Zr ₃₈ Ti ₅₃ V ₉	121.8	96.2	\	\	38.5	\
		Zr ₃₆ Ti ₅₂ V ₁₂	122.2	97.9	\	\	39.1	\
		Zr ₃₅ Ti ₅₀ V ₁₅	123.6	99.3	\	\	40.5	\

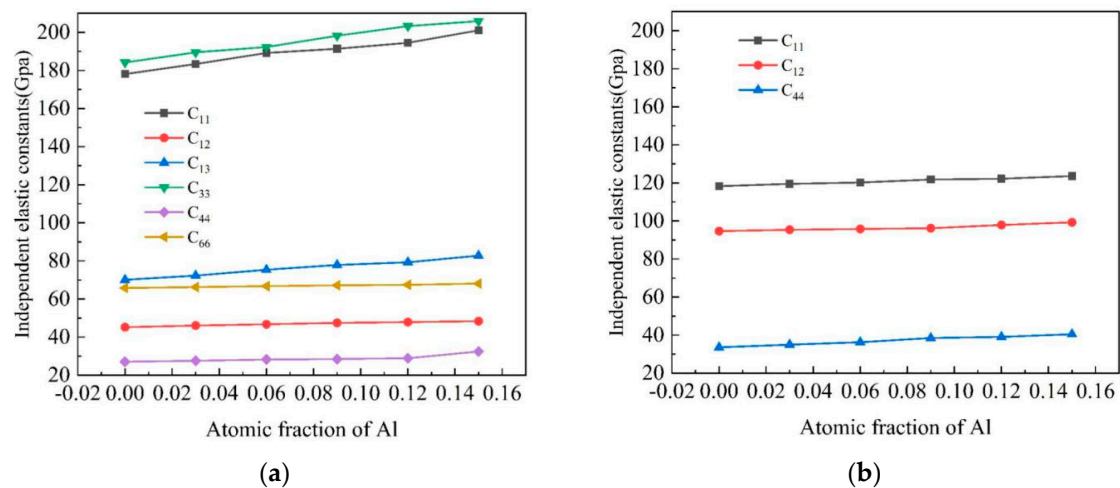


Figure 4. (a) Effect of Al atomic fraction on the independent elastic constants of HCP-structured Zr-Ti-Al alloy systems. (b) Effect of Al atomic fraction on the independent elastic constants of BCC-structured Zr-Ti-Al alloy systems.

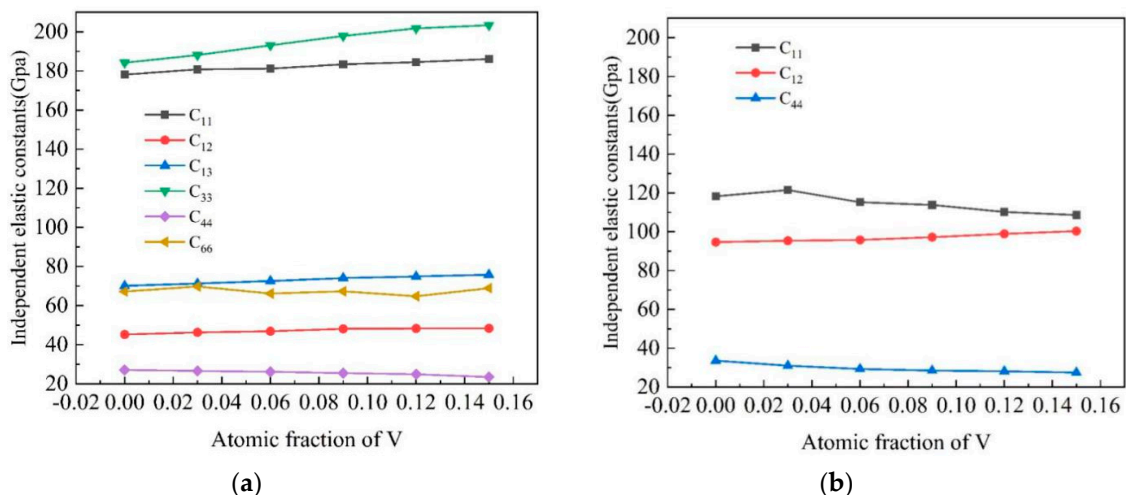


Figure 5. (a) Effect of V atomic fraction on the independent elastic constants of HCP-structured Zr-Ti-V alloy systems. (b) Effect of V atomic fraction on the independent elastic constants of BCC-structured Zr-Ti-V alloy systems.

As can be seen from Figures 4 and 5, in the calculated elastic constants of HCP Zr-Ti-Al alloys and HCP Zr-Ti-V alloys, C_{11} and C_{33} are much larger than other elastic constants, which shows that they are highly incompressible under uniaxial stress along the a and c axes. Moreover, as a hexagonal structure unit cell, the value of C_{33} is greater than the value of C_{11} , indicating that the c-axis of these materials is more difficult to compress than a-axis. In addition, it can be seen in Figures 4 and 5, the C_{44} of the HCP Zr-Ti-Al alloys is only about 28 GPa, and the C_{44} of the HCP Zr-Ti-V alloys is only about 25 GPa. These results indicate that HCP Zr-Ti-Al alloys and HCP Zr-Ti-V alloys have very weak resistance to shear deformation in the (100) plane.

In addition, for all Zr-Ti-Al alloys and Zr-Ti-V alloys constructed in this study, the Cauchy pressure calculated under the set environmental conditions is positive, which are generally higher than those of the Zr-Ti alloys [36]. These results indicate that these two alloy systems have higher ductility than Zr-Ti alloy systems, therefore, the introduction of alloying elements Al and V can improve the ductility of Zr-Ti alloy systems, and verified the experimental research results by Liang et al. [18,21].

Based on HCP structure and BCC structure, the elastic properties of the Zr-Ti-Al alloys of different Al atomic fractions and the Zr-Ti-V alloys of different V atomic fractions are calculated by first principles

in this paper, the calculation results using Equations (11)–(18) are shown in Tables 9 and 10, as well as Figures 6 and 7.

Table 9. Elastic properties of HCP structure and BCC structure Zr-Ti-Al alloy systems.

Structures	System	Composition (at.%)	Elastic Properties				
			B_H (GPa)	G_H (GPa)	B_H/G_H	E(GPa)	ν
HCP	Zr-Ti-Al	Zr ₄₁ Ti ₅₉	89.5	39.2	2.28	102.6	0.309
		Zr ₄₀ Ti ₅₇ Al ₃	91.9	40.2	2.29	105.3	0.309
		Zr ₃₉ Ti ₅₅ Al ₆	94.3	41.3	2.28	108.1	0.309
		Zr ₃₈ Ti ₅₃ Al ₉	95.5	41.7	2.29	109.2	0.309
		Zr ₃₆ Ti ₅₂ Al ₁₂	96.8	42.4	2.28	111	0.309
		Zr ₃₅ Ti ₅₀ Al ₁₅	99.3	46.1	2.15	120	0.299
BCC	Zr-Ti-Al	Zr ₄₁ Ti ₅₉	102.6	22.1	4.64	61.9	0.4
		Zr ₄₀ Ti ₅₇ Al ₃	103.4	22.8	4.53	63.7	0.397
		Zr ₃₉ Ti ₅₅ Al ₆	103.9	23.5	4.42	65.6	0.395
		Zr ₃₈ Ti ₅₃ Al ₉	104.7	24.8	4.22	69	0.39
		Zr ₃₆ Ti ₅₂ Al ₁₂	106.9	24.5	4.36	68.3	0.394
		Zr ₃₅ Ti ₅₀ Al ₁₅	107.4	25.1	4.27	69.9	0.392

Table 10. Elastic properties of HCP structure and BCC structure Zr-Ti-V alloy systems.

Structures	System	Composition (at.%)	Elastic Properties				
			B_H (GPa)	G_H (GPa)	B_H/G_H	E(GPa)	ν
HCP	Zr-Ti-V	Zr ₄₁ Ti ₅₉	89.5	39.2	2.28	102.6	0.309
		Zr ₄₀ Ti ₅₇ V ₃	91.1	35.1	2.60	93.3	0.292
		Zr ₃₉ Ti ₅₅ V ₆	91.7	38.6	2.38	101.6	0.315
		Zr ₃₈ Ti ₅₃ V ₉	93.4	38.1	2.45	100.6	0.320
		Zr ₃₆ Ti ₅₂ V ₁₂	93.7	37.8	2.47	100.0	0.322
		Zr ₃₅ Ti ₅₀ V ₁₅	94.3	36.9	2.56	98.0	0.327
BCC	Zr-Ti-V	Zr ₄₁ Ti ₅₉	102.6	22.1	4.64	61.9	0.400
		Zr ₄₀ Ti ₅₇ V ₃	104.1	20.0	5.21	56.6	0.410
		Zr ₃₉ Ti ₅₅ V ₆	102.3	16.2	6.31	46.2	0.425
		Zr ₃₈ Ti ₅₃ V ₉	102.7	17.4	7.13	41.3	0.433
		Zr ₃₆ Ti ₅₂ V ₁₂	102.6	15.0	6.84	42.9	0.431
		Zr ₃₅ Ti ₅₀ V ₁₅	103.1	13.3	7.75	38.3	0.438

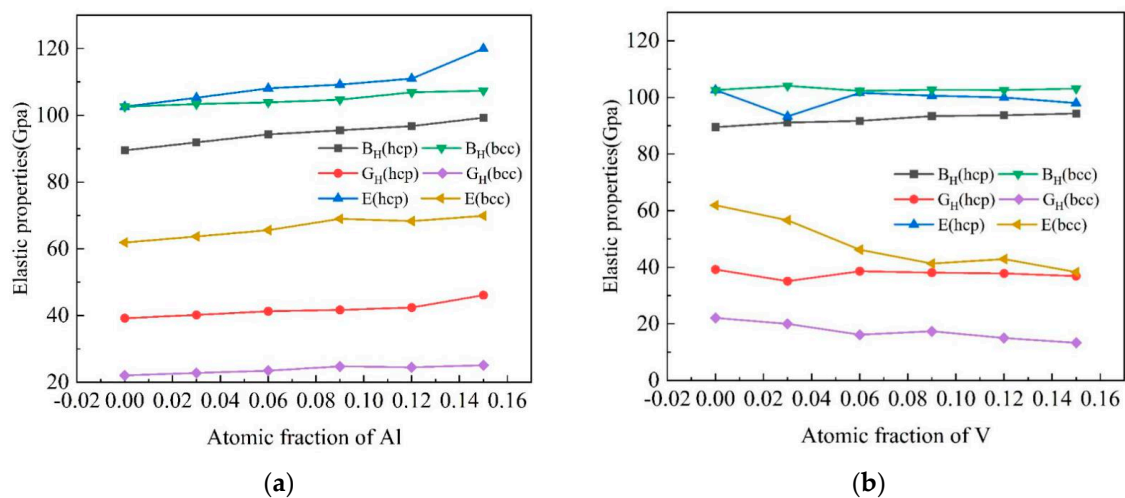


Figure 6. (a) Effect of Al atomic fraction on bulk modulus B_H , shear modulus G_H and Young’s modulus E of Zr-Ti-Al alloy system. (b) Effect of V atomic fraction on bulk modulus B_H , shear modulus G_H and Young’s modulus E of Zr-Ti-V alloy system.

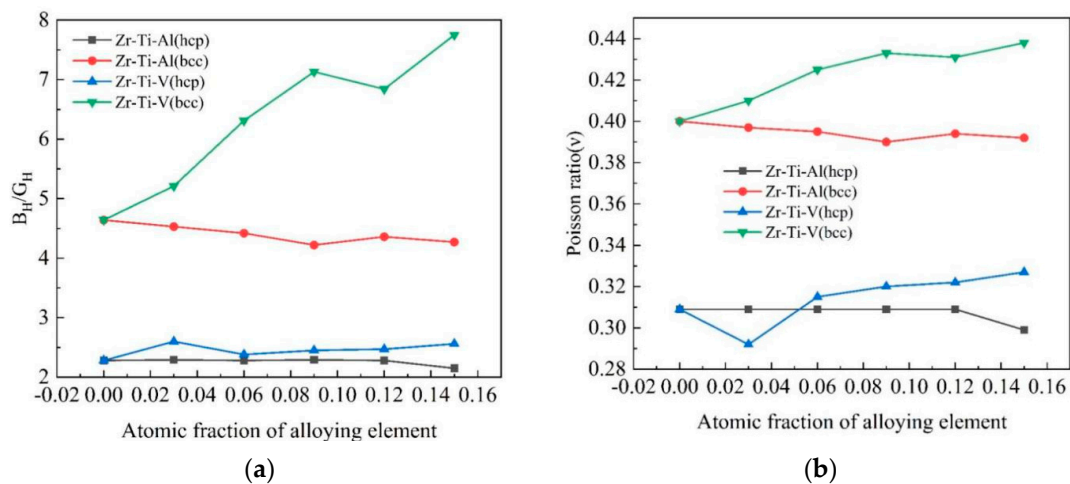


Figure 7. (a) Effect of Al atom fraction on B_H/G_H value of Zr-Ti-Al alloy system and effect of V atom fraction on B_H/G_H value of Zr-Ti-V alloy system. (b) Effect of Al atom fraction on Poisson's ratio of Zr-Ti-Al alloy system and effect of V atom fraction on Poisson's ratio of Zr-Ti-V alloy system.

For Zr-Ti-Al alloys, it can be seen from Figure 6a that the bulk modulus of the HCP structure is less than that of BCC, indicating that α phase of Zr-Ti-Al alloys is lower than that of β phase. However, the HCP Zr-Ti-Al alloys have higher shear modulus and Young's modulus than BCC, which indicates that the hardness and stiffness of α phase are higher than that of β phase. In addition, the bulk modulus, shear modulus, and Young's modulus of HCP-structured Zr-Ti-Al alloys are positively correlated with Al atomic fraction. When the mass fraction of Al increases between 0 and 6.8 wt.%, the strength, hardness, and stiffness of α phase in Zr-Ti-Al alloys will be improved with the increasing of Al. For BCC Zr-Ti-Al alloys, their bulk modulus, shear modulus, and Young's modulus are basically unchanged when the Al mass fraction exceeds 4 wt.%, and then these values continue to increase. In general, when the mass fraction of Al in the Zr-Ti-Al alloys is from 4 wt.% to 6.8 wt.%, the Zr-Ti-Al alloys have the highest strength, hardness, and rigidity.

As shown in Figure 6b, for the Zr-Ti-V alloys, the bulk modulus of the HCP structure are lower than that of BCC, which shows that the strength of α phase of Zr-Ti-V alloys is lower than that of β phase. In addition, the bulk modulus of HCP-structured Zr-Ti-V alloys is positively correlated with the atomic fraction of V, but the shear modulus and Young's modulus are negatively correlated. When the mass fraction of V increases from 0 to 12 wt.%, the strength of α phase in the Zr-Ti-V alloys will be improved, while the hardness and rigidity of them will be weakened.

With the increasing of atomic fraction of V, the bulk modulus of BCC Zr-Ti-V alloys increases first and then remains unchanged. When the mass fraction of V increases from 0 to 2.4 wt.%, the strength of β phase in the Zr-Ti-V alloys will be enhanced, and when the mass fraction of V exceeds 2.4 wt.%, the strength of β phase in the Zr-Ti-V alloys is basically unchanged with the increasing mass fraction of V. In addition, the shear modulus and Young's modulus of the BCC Zr-Ti-V alloys are negatively correlated with the element V, which indicates that the hardness and stiffness of β phase in Zr-Ti-V alloys will be reduced with the increasing of V element. In general, it can be seen that with the increasing of V mass fraction, the strength of Zr-Ti-V alloys improves, while the hardness and stiffness are opposite. When the mass fraction of V is around 2.4 wt.%, the Zr-Ti-V alloys achieve the best strength, hardness, and stiffness.

As shown in Figure 7, for Zr-Ti-Al alloys and Zr-Ti-V alloys, the B_H/G_H value of the BCC structure is greater than that of HCP. These two types of alloy systems have similar characteristics in Poisson's ratio, which indicates that the ductility of α phase is lower than that of β phase in Zr-Ti-Al alloys and Zr-Ti-V alloys. In addition, for HCP Zr-Ti-Al alloys, when the Al mass fraction is between 0 and 5.2 wt.%, the increasing of Al atomic fraction has almost no effect on the B_H/G_H value of the HCP Zr-Ti-Al alloys. However, the B_H/G_H value of the HCP structure Zr-Ti-Al alloys tends to decrease after

the Al mass fraction exceeds 5.2 wt.%, and the Poisson's ratio of the HCP Zr-Ti-Al alloys also follows a similar rule. For BCC Zr-Ti-Al alloys, the increase of Al atomic fraction will reduce the B_H/G_H value and Poisson's ratio of these alloy systems. It can be concluded that with the increasing of the Al mass fraction, the ductility of the β phase of the Zr-Ti-Al alloys will be weakened. On the contrary, for the Zr-Ti-V alloy systems, the ductility of these alloys will be improved as the V atomic fraction increases by observing the B_H/G_H value and Poisson's ratio in Figure 7, which indicates that the ductility of Zr-Ti-V alloys will be enhanced when the mass fraction of V increases from 0 to 12 wt.%.

In this paper, we studied the influence of Zr and Ti on the phase composition of ternary Zr-Ti-X alloys ($X = \text{Al}, \text{V}$) by the content of different Al and V. In addition, based on the research that the changes of phase compositions and structure with alloying element content distinctly affect the mechanical properties of quaternary Zr-Ti-Al-V alloys, first-principles calculations could provide an effective guide for further exploring the effects of the amount of Zr and Ti on the phase composition and structure of quaternary Zr-Ti-Al-V alloys, thereby providing direction and help in discussing the relationship between Zr-Ti-X ($X = \text{Al}, \text{V}$) compositions and the mechanical properties of the multiphase $\text{Zr}_{47}\text{Ti}_{45}\text{Al}_5\text{V}_3$ alloy.

4. Conclusions

To improve our fundamental understanding of the roles of alloying elements in Zr-Ti-X alloys ($X = \text{Al}, \text{V}$), first-principles calculations were performed with the SQS method to consider the disordered atomic configurations in solid solution alloys. In this paper, the relationship between the microstructure and properties of the Zr-Ti-X alloys ($X = \text{Al}, \text{V}$) is studied on the basis of $\text{Zr}_{47}\text{Ti}_{45}\text{Al}_5\text{V}_3$ (wt.%) alloy, based on a certain ratio of Zr and Ti atomic fractions, the effects of different alloying elements (Al, V) mass fractions and different phase structures (HCP and BCC structure, α phase and β phase) on the lattice stability and elastic properties of Zr-Ti-X alloys ($X = \text{Al}, \text{V}$) are calculated by the first principles. The main conclusions are as follows.

1. Al acts as an α stabilizer for Zr-Ti-Al alloys and V can stabilize the β phase for Zr-Ti-V alloys.
2. For Zr-Ti-Al alloy systems, the strength of α phase is lower than that of β phase, but the hardness and stiffness of the α phase are higher than that of β phase. For Zr-Ti-V alloy systems, the hardness and stiffness of α phase are higher than that of β phase, while the ductility of β phase is generally higher than that of α phase.
3. When the mass fraction of Al in Zr-Ti-Al alloys increases from 4 wt.% to 6.8 wt.%, Zr-Ti-Al alloys have relatively good strength, hardness, and rigidity, however, the ductility of Zr-Ti-Al alloys becomes worse as the mass fraction of Al increases. When the mass fraction of V in Zr-Ti-V alloys reaches 2.4 wt.%, Zr-Ti-V alloy achieves the best strength, hardness, and rigidity, and the ductility of Zr-Ti-V alloys improved as the mass fraction of V increases from 0 to 12 wt.%.
4. Mechanical properties of quaternary $\text{Zr}_{47}\text{Ti}_{45}\text{Al}_5\text{V}_3$ alloy significantly depend on the amount of Zr and Ti; in addition, the changes of phase compositions and structure with Al content or V content distinctly affect mechanical properties of ternary Zr-Ti-X alloys ($X = \text{Al}, \text{V}$), thereby impacting the mechanical properties of the multiphase $\text{Zr}_{47}\text{Ti}_{45}\text{Al}_5\text{V}_3$ alloy from the point of view of the amount of Zr and Ti.

Author Contributions: W.D. and X.Y. contributed equally to research and wrote the paper; X.L. contributed to the review and editing; Y.W. and B.L. contributed to resources. All authors have read and agreed to the published version of the manuscript.

Funding: This work was supported by the National Natural Science Foundation of China (Grant No. 51531005, Grant No. 51571174 and Grant No. 51421001) and the Fundamental Research Funds for the Central Universities of China (Project No. 106112017CDJQJ138803).

Conflicts of Interest: The authors declare no conflict of interest.

References

1. Alifanov, O.M.; Budnik, S.A.; Nenarokomov, A.; Netelev, A.; Titov, D.M. Destructive materials thermal characteristics determination with application for spacecraft structures testing. *Acta Astronaut.* **2013**, *85*, 113–119. [[CrossRef](#)]
2. Goebel, J.; Ghidini, T.; Graham, A. Stress-corrosion cracking characterisation of the advanced aerospace Al–Li 2099-T86 alloy. *Mater. Sci. Eng. A* **2016**, *673*, 16–23. [[CrossRef](#)]
3. Pradeep, T.; Soni, S.K.; Thomas, B. Design manufacture and testing of a composite support structure for spacecraft application. *Mater. Today Proc.* **2020**, *22*, 1374–1379. [[CrossRef](#)]
4. Catauro, M.; Mozzati, M.C.; Bollino, F. Sol–gel hybrid materials for aerospace applications: Chemical characterization and comparative investigation of the magnetic properties. *Acta Astronaut.* **2015**, *117*, 153–162. [[CrossRef](#)]
5. Lin, Y.; Tang, Y.; Zhang, X.-Y.; Chen, C.; Yang, H.; Zhou, K.-C. Effects of solution temperature and cooling rate on microstructure and micro-hardness of a hot compressed Ti-6Al-4V alloy. *Vacuum* **2019**, *159*, 191–199. [[CrossRef](#)]
6. Balasundar, I.; Ravi, K.; Raghu, T. On the high temperature deformation behaviour of titanium alloy BT3-1. *Mater. Sci. Eng. A* **2017**, *684*, 135–145. [[CrossRef](#)]
7. Zhao, Q.; Yang, F.; Torrens, R.; Bolzoni, L. Evaluation of the hot workability and deformation mechanisms for a metastable beta titanium alloy prepared from powder. *Mater. Charact.* **2019**, *149*, 226–238. [[CrossRef](#)]
8. Kumar, K.B.; Saxena, K.K.; Dey, S.R.; Pancholi, V.; Bhattacharjee, A. Peak stress studies of hot compressed TiHy 600 alloy. *Mater. Today Proc.* **2017**, *4*, 7365–7374. [[CrossRef](#)]
9. Bobbili, R.; Madhu, V. Constitutive modeling and fracture behavior of a biomedical Ti–13Nb–13Zr alloy. *Mater. Sci. Eng. A* **2017**, *700*, 82–91. [[CrossRef](#)]
10. Gu, X.; Dong, C.; Cheng, T. MPM simulations of high-speed machining of Ti6Al4V titanium alloy considering dynamic recrystallization phenomenon and thermal conductivity. *Appl. Math. Model.* **2018**, *56*, 517–538. [[CrossRef](#)]
11. Bagaber, S.; Abdullahi, T.; Harun, Z.; Daib, N.; Othman, M.H.D. The Effect of Lanthanum Addition on the Microstructure and Mechanical Properties of A390 Aluminium Alloy. *Arab. J. Sci. Eng.* **2017**, *62*, 23–4564. [[CrossRef](#)]
12. Liao, Z.; Luan, B.; Zhang, X.; Liu, R.; Murty, K.L.; Liu, Q. The effects of increasing deformation strain on the microstructural evolution of a metastable β -Zr alloy. *J. Alloys Compd.* **2019**, *800*, 208–218. [[CrossRef](#)]
13. Sandlöbes, S.; Korte-Kerzel, S.; Raabe, D. On the influence of the heat treatment on microstructure formation and mechanical properties of near- α Ti-Fe alloys. *Mater. Sci. Eng. A* **2019**, *748*, 301–312. [[CrossRef](#)]
14. Mironov, S.; Sato, Y.; Kokawa, H. Friction-stir welding and processing of Ti-6Al-4V titanium alloy: A review. *J. Mater. Sci. Technol.* **2018**, *34*, 58–72. [[CrossRef](#)]
15. Jing, R.; Liang, S.; Liu, C.; Ma, M.; Zhang, X.; Liu, R. Structure and mechanical properties of Ti-6Al-4V alloy after zirconium addition. *Mater. Sci. Eng. A* **2012**, *552*, 295–300. [[CrossRef](#)]
16. Liang, S.; Ma, M.; Jing, R.; Zhang, X.; Liu, R. Microstructure and mechanical properties of hot-rolled ZrTiAlV alloys. *Mater. Sci. Eng. A* **2012**, *532*, 1–5. [[CrossRef](#)]
17. Liang, S.; Yin, L.; Ma, M.; Jing, R.; Yu, P.; Zhang, Y.; Wang, B.; Liu, R. A multi-component Zr alloy with comparable strength and Higher plasticity than Zr-based bulk metallic glasses. *Mater. Sci. Eng. A* **2013**, *561*, 13–16. [[CrossRef](#)]
18. Liang, S.; Yin, L.; Che, H.; Jing, R.; Zhou, Y.; Ma, M.; Liu, R. Effects of Al content on structure and mechanical properties of hot-rolled ZrTiAlV alloys. *Mater. Des.* **2013**, *52*, 246–250. [[CrossRef](#)]
19. Zhang, P.-L.; Gong, Z.-Z.; Ji, G.-F.; Wang, Q.-S.; Song, Z.-F.; Cao, Y.; Wang, X. Shock Compression of the New 47Zr45Ti5Al3V Alloys up to 200 GPa. *Chin. Phys. Lett.* **2013**, *30*, 066401. [[CrossRef](#)]
20. Tan, Y.; Ji, L.; Duan, J.; Liu, W.; Zhang, J.; Liu, R. A Study on the Hot Deformation Behavior of 47Zr-45Ti-5Al-3V Alloy with Initial Lamellar α Structure. *Met. Mater. Trans. A* **2016**, *47*, 5974–5984. [[CrossRef](#)]
21. Liang, S.; Feng, Z.; Yin, L.; Liu, X.; Ma, M.; Liu, R. The effects of V content on the microstructure and mechanical properties of hot rolled TiZr based alloys. *J. Alloys Compd.* **2016**, *664*, 11–18. [[CrossRef](#)]
22. Tan, Y.B.; Ji, L.-Y.; Liu, W.-C.; Xiang, S.; Zhao, F.; Liang, Y.-L. Effect of hot deformation on $\alpha \rightarrow \beta$ phase transformation in 47Zr-45Ti-5Al-3V alloy. *Trans. Nonferrous Met. Soc. China* **2018**, *28*, 1947–1957. [[CrossRef](#)]

23. Liang, S.; Yin, L.; Zheng, L.; Ma, M.; Liu, R. Microstructure and Mechanical Properties of Graphite Mold Casted TiZrAlV Alloy with Various Zr Contents. *Adv. Eng. Mater.* **2016**, *18*, 1581–1587. [[CrossRef](#)]
24. Zhng, C.X.; Wang, L.M.; Liu, R.P.; Zhao, B.J.; Luo, J.T. ZrTiAlV alloy grain refining under high-pressure torsion and electric field-assisted heat treatment. *Mater. Charact.* **2017**, *127*, 231–238. [[CrossRef](#)]
25. Tan, Y.; Yang, L.; Duan, J.; Ji, L.; Liu, W. Studies on the kinetics of $\beta \rightarrow \alpha$ phase transformation in 47Zr–45Ti–5Al–3V alloy under isothermal conditions by X-ray diffraction. *Mater. Charact.* **2016**, *112*, 98–104. [[CrossRef](#)]
26. Bekker, T.B.; Litasov, K.; Shatskiy, A.; Sagatov, N.; Krinitsin, P.; Krasheninnikov, S.; Podborodnikov, I.; Rashchenko, S.V.; Davydov, A.; Ohfujii, H. Towards the investigation of ternary compound in the Ti–Al–Zr–O system: Effect of oxygen fugacity on phase formation. *J. Eur. Ceram. Soc.* **2020**, *40*, 3663–3672. [[CrossRef](#)]
27. Chen, W.; Jia, Y.; Yi, J.; Wang, M.; Derby, B.; Lei, Q. Effect of addition of Ni and Si on the microstructure and mechanical properties of Cu–Zn alloys. *J. Mater. Res.* **2017**, *32*, 3137–3145. [[CrossRef](#)]
28. Zhu, J.; Kamiya, A.; Yamada, T.; Shi, W.; Naganuma, K. Influence of boron addition on microstructure and mechanical properties of dental cast titanium alloys. *Mater. Sci. Eng. A* **2003**, *339*, 53–62. [[CrossRef](#)]
29. Wang, J.; Zheng, W.; Xu, G.; Zeng, X.; Cui, Y. Thermodynamic assessment of the Ti–Al–Zr system and atomic mobility of its bcc phase. *Calphad* **2020**, *70*, 101801. [[CrossRef](#)]
30. Kirnbauer, A.; Kretschmer, A.; Koller, C.; Wojcik, T.; Paneta, V.; Hans, M.; Schneider, J.; Polcik, P.; Mayrhofer, P. Mechanical properties and thermal stability of reactively sputtered multi-principal-metal Hf-Ta-Ti-V-Zr nitrides. *Surf. Coat. Technol.* **2020**, *389*, 125674. [[CrossRef](#)]
31. Tang, P.; Li, W.; Zhao, Y.; Wang, K.; Li, W.; Zhan, F. Influence of strontium and lanthanum simultaneous addition on microstructure and mechanical properties of the secondary Al–Si–Cu–Fe alloy. *J. Rare Earths* **2017**, *35*, 485–493. [[CrossRef](#)]
32. Zhou, Y.-K.; Jing, R.; Ma, M.-Z.; Liu, R.; Yun-Kai, Z.; Ran, J.; Ming-Zhen, M.; Ri-Ping, L. Tensile Strength of Zr–Ti Binary Alloy. *Chin. Phys. Lett.* **2013**, *30*, 116201. [[CrossRef](#)]
33. Marker, C.; Shang, S.-L.; Zhao, J.-C.; Liu, Z.-K. Elastic knowledge base of bcc Ti alloys from first-principles calculations and CALPHAD-based modeling. *Comput. Mater. Sci.* **2017**, *140*, 121–139. [[CrossRef](#)]
34. Liao, M.; Liu, Y.; Cui, P.; Qu, N.; Zhou, F.; Yang, D.; Han, T.; Lai, Z.; Zhu, J. Modeling of alloying effect on elastic properties in BCC Nb–Ti–V–Zr solid solution: From unary to quaternary. *Comput. Mater. Sci.* **2020**, *172*, 109289. [[CrossRef](#)]
35. Konopatsky, A.; Dubinskiy, S.; Zhukova, Y.; Sheremetyev, V.; Brailovski, V.; Prokoshkin, S.; Filonov, M. Ternary Ti–Zr–Nb and quaternary Ti–Zr–Nb–Ta shape memory alloys for biomedical applications: Structural features and cyclic mechanical properties. *Mater. Sci. Eng. A* **2017**, *702*, 301–311. [[CrossRef](#)]
36. Yang, X.G.; Liang, X.P.; Wang, Y.; Luan, B.F. First-principles Study on Phase Stability and Elastic Properties of Zr–Ti Alloy. *Rare Met. Mater. Eng. China* **2020**, *49*, 2004–2010.
37. Kohn, W.; Sham, L.J. Quantum Density Oscillations in an Inhomogeneous Electron Gas. *Phys. Rev.* **1965**, *137*, A1697–A1705. [[CrossRef](#)]
38. Clark, S.J.; Segall, M.D.; Pickard, C.J.; Hasnip, P.J.; Probert, M.I.J.; Refson, K.; Payne, M.C. First principles methods using CASTEP. *Cryst. Mater.* **2005**, *220*, 5–6. [[CrossRef](#)]
39. Fang, H.; Gu, M.; Liu, B.; Liu, X.; Huang, S.; Ni, C.; Li, Z.; Wang, R. Plane-wave pseudopotential study for the structural stability of Hf: The role of spin–orbit interaction. *Phys. B Condens. Matter* **2011**, *406*, 1744–1748. [[CrossRef](#)]
40. Kong, X.-S.; Wu, X.; You, Y.-W.; Liu, C.; Fang, Q.; Chen, J.-L.; Luo, G.-N.; Wang, Z. First-principles calculations of transition metal–solute interactions with point defects in tungsten. *Acta Mater.* **2014**, *66*, 172–183. [[CrossRef](#)]
41. Muzyk, M.; Nguyen-Manh, D.; Kurzydłowski, K.J.; Baluc, N.L.; Dudarev, S.L. Phase stability, point defects, and elastic properties of W–V and W–Ta alloys. *Phys. Rev. B* **2011**, *84*, 104115. [[CrossRef](#)]
42. Hu, Y.-J.; Shang, S.-L.; Wang, Y.; Darling, K.A.; Butler, B.G.; Kecskes, L.J.; Liu, Z.-K. Effects of alloying elements and temperature on the elastic properties of W-based alloys by first-principles calculations. *J. Alloys Compd.* **2016**, *671*, 267–275. [[CrossRef](#)]
43. Giusepponi, S.; Celino, M. The ideal tensile strength of tungsten and tungsten alloys by first-principles calculations. *J. Nucl. Mater.* **2013**, *435*, 52–55. [[CrossRef](#)]

44. Muzyk, M.; Nguyen-Manh, D.; Wrobel, J.; Kurzydłowski, K.J.; Baluc, N.; Dudarev, S. First-principles model for phase stability, radiation defects and elastic properties of W-Ta and W-V alloys. *J. Nucl. Mater.* **2013**, *442*, S680–S683. [[CrossRef](#)]
45. Wei, N.; Jia, T.; Zhang, X.; Liu, T.; Zeng, Z.; Yang, X. First-principles study of the phase stability and the mechanical properties of W-Ta and W-Re alloys. *AIP Adv.* **2014**, *4*, 057103. [[CrossRef](#)]
46. Bertoldi, D.S.; Ramos, S.B.; Guillermet, A.F. Interrelations between EOS parameters and cohesive energy of transition metals: Thermostatistical approach, ab initio calculations and analysis of “universality” features. *J. Phys. Chem. Solids* **2017**, *107*, 93–99. [[CrossRef](#)]
47. Perdew, J.P.; Ruzsinszky, A.; Csonka, G.I.; Vydrov, O.A.; Scuseria, G.E.; Constantin, L.A.; Zhou, X.; Burke, K. Restoring the Density-Gradient Expansion for Exchange in Solids and Surfaces. *Phys. Rev. Lett.* **2008**, *100*, 136406. [[CrossRef](#)]
48. Pokluda, J.; Cerny, M.; Sob, M.; Umeno, Y. Ab initio calculations of mechanical properties: Methods and applications. *Prog. Mater. Sci.* **2015**, *73*, 127–158. [[CrossRef](#)]
49. Mehl, M.J.; Klein, B.M.; Papaconstantopoulos, D.A. First Principles Calculations of Elastic Properties of Metals. *Intermet. Compd. Princ. Pract.* **1994**, *1*, 195–210.
50. Zhou, W.; Sahara, R.; Tsuchiya, K. First-principles study of the phase stability and elastic properties of Ti-X alloys (X = Mo, Nb, Al, Sn, Zr, Fe, Co, and O). *J. Alloys Compd.* **2017**, *727*, 579–595. [[CrossRef](#)]
51. Voigt, W. Ueber die Beziehung zwischen den beiden Elasticitätsconstanten isotroper Körper. *Ann. der Phys.* **1889**, *274*, 573–587. [[CrossRef](#)]
52. Reuss, A. Berechnung der fliegrenze von mischkristallen auf grund der plastizittsbedingung für einkristalle. *J. Appl. Math. Mech.* **1929**, *9*, 49–58.
53. Hill, R. The Elastic Behaviour of a Crystalline Aggregate. *Proc. Phys. Soc. Sect. A* **1952**, *65*, 349–354. [[CrossRef](#)]
54. Hill, R. Elastic properties of reinforced solids: Some theoretical principles. *J. Mech. Phys. Solids* **1963**, *11*, 357–372. [[CrossRef](#)]
55. Pugh, S. XCII. Relations between the elastic moduli and the plastic properties of polycrystalline pure metals. *Philos. Mag. J. Sci.* **1954**, *45*, 823–843. [[CrossRef](#)]
56. Vitos, L.; Korzhavyi, P.A.; Johansson, B. Elastic Property Maps of Austenitic Stainless Steels. *Phys. Rev. Lett.* **2002**, *88*, 155501. [[CrossRef](#)]
57. Vijh, A. The pitting corrosion potentials of metals and surface alloys in relation to their solid state cohesion. *Mater. Chem. Phys.* **1988**, *20*, 371–380. [[CrossRef](#)]
58. Li, X.; Zhao, J.; Xu, J.; Liu, X. Mechanical Properties and Defective Effects of 316LN Stainless Steel by First-Principles Simulations. *J. Mater. Sci. Technol.* **2011**, *27*, 1029–1033. [[CrossRef](#)]
59. Clerc, D.G. Mechanical Hardness: Atomic-level Calculations for Diamond-like Materials. *J. Mater. Sci. Lett.* **1998**, *17*, 1461–1462. [[CrossRef](#)]
60. Reeh, S.; Music, D.; Ekholm, M.; Abrikosov, I.A.; Schneider, J.M. Elastic properties of fcc Fe-Mn-X (X=Cr, Co, Ni, Cu) alloys from first-principles calculations. *Phys. Rev. B* **2013**, *87*, 224103. [[CrossRef](#)]
61. Xu, J.; Zhao, J.; Korzhavyi, P.A.; Johansson, B. Ab initio calculations of elastic properties of Fe–Cr–W alloys. *Comput. Mater. Sci.* **2014**, *84*, 301–305. [[CrossRef](#)]
62. Pettifor, D.G. Theoretical predictions of structure and related properties of intermetallics. *Mater. Sci. Technol.* **1992**, *8*, 345–349. [[CrossRef](#)]
63. Jiang, D.; Wu, M.; Liu, D.; Li, F.; Chai, M.; Liu, S. Structural Stability, Electronic Structures, Mechanical Properties and Debye Temperature of Transition Metal Impurities in Tungsten: A First-Principles Study. *Metals* **2019**, *9*, 967. [[CrossRef](#)]
64. Cordeiro, J.; Barão, V.A.R. Is there scientific evidence favoring the substitution of commercially pure titanium with titanium alloys for the manufacture of dental implants? *Mater. Sci. Eng. C* **2017**, *71*, 1201–1215. [[CrossRef](#)] [[PubMed](#)]

